Compressive Cooperative Sensing and Mapping in Mobile Networks

Yasamin Mostofi, *Member*, *IEEE*

Abstract—In this paper, we consider a mobile cooperative network that is tasked with building a map of the spatial variations of a parameter of interest, such as an obstacle map or an aerial map. We propose a new framework that allows the nodes to build a map of the parameter of interest with a small number of measurements. By using the recent results in the area of compressive sensing, we show how the nodes can exploit the sparse representation of the parameter of interest in the transform domain in order to build a map with *minimal sensing*. The proposed work allows the nodes to efficiently map the areas that are not sensed directly. We consider three main areas essential to the cooperative operation of a mobile network: building a map of the spatial variations of a field of interest such as aerial mapping, mapping of the obstacles based on only wireless measurements, and mapping of the communication signal strength. For the case of obstacle mapping, we show how our framework enables a novel *noninvasive* mapping approach (without direct sensing), by using wireless channel measurements. Overall, our results demonstrate the potentials of this framework.

Index Terms—Mobile networks, compressive sensing, cooperative spatial mapping, mapping of obstacles, mapping of communication signal strength.

1 Introduction

Mobile intelligent networks can play a key role in emergency response, surveillance and security, and battlefield operations. The vision of a multiagent robotic network cooperatively learning and adapting in harsh unknown environments to achieve a common goal is closer than ever. In this paper, we are interested in the cases where a mobile cooperative network is tasked with collecting information from its environment. More specifically, we consider scenarios where the network is in charge of building a map of the spatial variations of a parameter (or a number of parameters) cooperatively, to which we refer to as **cooperative mapping**. Such problems can arise in several different applications. For instance, building a map of the indoor obstacles [3], ocean sampling [4], or aerial mapping [5] all fall into this category. A mobile network tasked with a certain exploratory mission faces an abundance of information. In such an information-rich world, there is simply not enough time to sample the whole environment due to the potential delay-sensitive nature of the application as well as other practical constraints. A group of Unmanned Air Vehicles (UAVs), for instance, may need to cooperatively build an aerial map of an area in a limited time, as is shown in Fig. 1. It is not practical to wait for the collective sampling of the vehicles to cover every single point in the terrain. A fundamental open question is then as follows: *What is the minimal collective sensing needed to accurately build a map of the whole terrain despite the fact that significant parts of it will not be sampled*? This is a considerably important problem as it enhances our ability to collect information and allows us to keep up with the high volume of information in the environment.

If we can understand the core information present in the data and can show that it has a dimension far less than the data itself, we can then reduce our sensing considerably. While considerable progress has been made in the area of mobile networks, a framework that allows the vehicles to reconstruct the parameter of interest based on a severely under-determined data set is currently missing. In most related work, only areas that are directly sensed are mapped. The rich literature on Simultaneous Localization and Mapping (SLAM) and its several variations fall into this category [6], [7], [8], [9]. SLAM approaches mainly focus on reducing the uncertainty in the sensed landmarks by using a Kalman filter. Similarly, approaches based on generating an occupancy map also address sensing uncertainty [10]. Another set of approaches, suitable mainly for mapping obstacles, are based on the Next Best View (NBV) problem [3], [11], [12], [13], [14]. In NBV approaches, the aim is to move to the positions "good" for sensing by guiding the vehicles to the perceived next safest area (area with the most visibility) based on the current map [3]. However, areas that are not sensed directly are not mapped in NBV. In [16], it is assumed that the spatial field of interest has a Gaussian distribution with known models for its average and autocorrelation. Similarly, in [4] and [17], a linear estimator is used based on known first and second order statistics of the field. In practice, however, spatial models of the average and autocorrelation of the field may not be available. Therefore, such approaches may not be suitable for developing a framework for mapping based on minimal sensing and without a priori information on field distribution.

• *The author is with the Department of Electrical and Computer Engineering, University of New Mexico, MSC01 1100, 1 University of New Mexico, Albuquerque, NM 87131-0001.*
E-mail: ymostofi@ece.unm.edu.

Manuscript received 14 Mar. 2010; revised 1 Oct. 2010; accepted 2 Dec. 2010; published online 9 Feb. 2011.
For information on obtaining reprints of this article, please send e-mail to: tmc@computer.org, and reference IEEECS Log Number TMC-2010-03-0123. Digital Object Identifier no. 10.1109/TMC.2011.31.

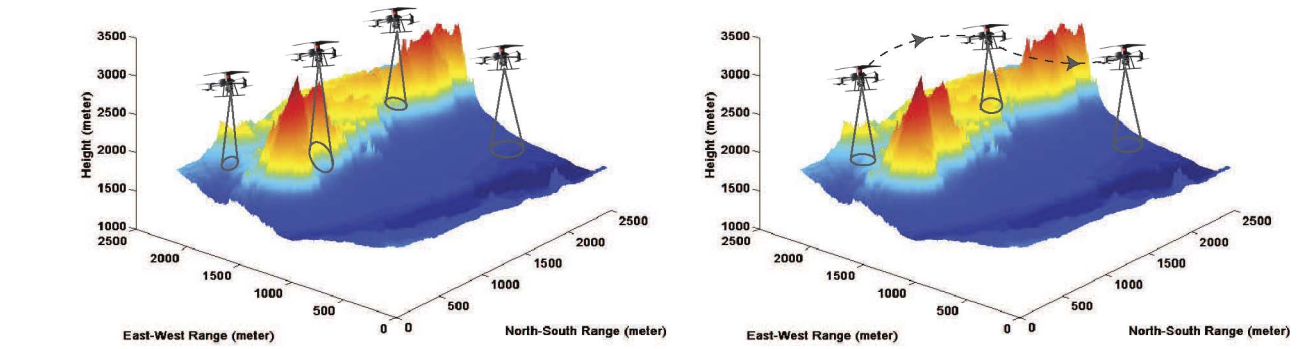

Fig. 1. An example of cooperative sensing and mapping: (left) a group of Unmanned Aerial Vehicles need to build a map of the spatial variations of Sandia Mountains in New Mexico with minimal sensing and (right) a single UAV is making measurements across its trajectory for either solo reconstruction or as part of a group mapping (data courtesy of US Geological Survey [26]).

In this paper, we present a *compressive cooperative mapping* framework for mobile exploratory networks, by extending our previous work [1], [2]. By compressive cooperative mapping, we refer to the cooperative mapping of a spatial function based on a considerably small observation set where a large percentage of the area of interest is not sensed directly. Our proposed theory and design tools are inspired by the recent breakthroughs in nonuniform sampling theory [18], [19]. The famous Nyquist-Shannon sampling theorem [20] revolutionized several different fields by showing that, under certain conditions, it is indeed possible to reconstruct a uniformly sampled signal perfectly. The new theory of *compressive sampling* (also known by other terms such as compressed sensing, compressive sensing or sparse sensing) shows that under certain conditions, it is possible to reconstruct a signal from a considerably incomplete set of observations, i.e., with a number of measurements much less than predicted by the Nyquist-Shannon theorem [18], [19]. This opens new and fundamentally different possibilities in terms of information gathering and processing in mobile networks. In this paper, we develop the fundamentals of cooperative sensing and mapping in mobile networks from a compressive sampling perspective.

While our proposed framework would be applicable to several mobile network applications, in this paper we focus on three main areas essential to the efficient and robust operation of a cooperative network. A mobile network is given an exploratory task, such as *collective ground, aerial, or underwater mapping*. It furthermore needs to *maintain connectivity*. In order to do so, an estimation of the spatial variations of the communication signal strength becomes crucial. Finally, it needs to *build a map of the obstacles* for navigation. Fig. 1 shows an example of cooperative aerial mapping. We show how our proposed framework can impact these three key areas, resulting in cooperative mapping with minimal sensing. In the area of obstacle mapping, we furthermore propose a novel way of mapping obstacles *noninvasively*, i.e., without sensing them directly. By using wireless channel measurements and the compressive mapping framework, we show how the robots can map the obstacles before entering a building or a room. A survey of the existing work in the literature shows very few papers that use wireless measurements for obstacle mapping. There are, however, a number of papers on detecting an object, using fixed sensors [21], [22], [23], [24]. For instance, in [23], the authors build a network of several hundred fixed sensors in order to detect presence of a person. The framework is based on making several measurements between pairs of sensors, as opposed to a very small number of measurements. Then the goal is to roughly track a person instead of building a map of the obstacles. There is a need for prior learning in the area of interest as well. As such, the work of Wilson and Patwari [23] is on detecting an obstruction to a wireless signal as opposed to obstacle mapping with minimal measurements. It should also be noted that a detection case can be considered as a simplified version of obstacle mapping, where the details do not matter. As such, our proposed framework can also improve the detection performance of the aforementioned papers.

While we use the term "cooperative mapping" throughout the paper, most of the proposed framework is also applicable to the case where only one robot is tasked with building a spatial map of a field of interest. The paper is organized as follows: In Section 2, we discuss the compressibility of the signals of interest in mobile exploratory networks. In Section 3, we provide a brief introduction to the theory of compressive sensing. In Section 4, we consider cooperative aerial mapping, mapping of obstacles as well as mapping of the spatial variations of the communication signal strength. In particular, we propose a novel compressive and noninvasive technique for mapping of the obstacles, based on wireless channel measurements. We conclude in Section 5. A list of key variables used in the paper is provided in Table 1.

2 Signal Compressibility in Cooperative Mobile Networks

We first define what "sparse" and "compressible" signals refer to.

Definition. *A* sparse *signal is a signal that can be represented with a small number of nonzero coefficients.*

Definition. *A* compressible *signal is a signal that has a transformation where most of its energy is in a very few coefficients, making it possible to approximate the rest with zero. In this paper, we are interested in linear transformations.*

TABLE 1
Key Notations Used in This Paper

N	size of the original signal in the primal domain
S	size of the support of the signal in the sparse domain
K	number of measurements taken to estimate the signal
x	signal in the primal domain, an $N \times 1$ vector
y	$K \times 1$ measured vector of x in the primal domain
X	$N \times 1$ vector representing a linear transform of x
Φ	$K \times N$ observation matrix, s.t. $y = \Phi x$
Γ	$N \times N$ linear projection matrix, s.t. $x = \Gamma X$
Γ^H	Hermitian of Γ
Ψ	$K \times N$ matrix (defined as $\Psi = \Phi \times \Gamma$), s.t. $y = \Psi X$

The new theory of compressive sampling shows that, under certain conditions, a compressible signal can be reconstructed using very few observations. Most natural signals are indeed compressible. The best sparse representation of a signal depends on the application and can be inferred from analyzing similar data. Our analysis of aerial maps, obstacle maps (indoor or outdoor) as well as maps of communication signal strength, for instance, has shown them to have a considerably sparse representation. Fig. 2 shows two maps based on real data, an aerial map, and an obstacle map. By applying a linear transformation to the signals (Fourier to the left signal and wavelet to the right one), it can be seen that most of the signal's energy is contained in a small percentage of the transform coefficients. For instance, 100 percent of the energy is in less than 1 percent of the wavelet coefficients for the obstacle map on the right. However, this energy is not necessarily confined to a consecutive set of transform coefficients, which makes reconstructing the signal based on a considerably small number of observations challenging. In general, Fourier transformation can provide a good compression for the spatial variations of the communication channel or a height map. For an obstacle map (see Fig. 2b), wavelet transform or total variation (a difference-based approach) can provide an even better compression. It should be noted that in the compressive mapping of the obstacles, we do not consider an object-based approach. Instead, we consider the space of interest as a binary spatial function that takes on values of 0 or 1. It is also possible to make it nonbinary and include the properties of the objects as we shall see in Section 4.2.

In this paper, we show how the new theory of compressive sampling can result in fundamentally different sensing approaches in mobile cooperative exploratory networks. While several signals of interest to the operation of a mobile network have sparse representations, the main challenge is to sense them in the right domain such that it is possible to reconstruct them with minimal sensing, as we show in the next sections. For instance, an obstacle map is sparse in the spatial domain. However, by directly point-sampling it in the spatial domain, it will not be possible to reconstruct it with a very small number of observations. Therefore, new sensing methods are required, as we will propose in the next sections.

3 Overview of Compressive Sampling Theory

The new theory of sampling is based on the fact that real-world signals typically have a sparse representation in a certain transformed domain. Exploiting sparsity, in fact, has a rich history in different fields. For instance, it can result in reduced computational complexity (such as in matrix calculations) or better compression techniques (such as in JPEG2000). However, in such approaches, the signal of interest is first fully sampled, after which a transformation is applied and only the coefficients above a certain threshold are saved. This, however, is not efficient as it puts a heavy burden on sampling the entire signal when only a small percentage of the transformed coefficients are needed to represent it. The new theory of compressive sampling, on the other hand, allows us to sense the signal in a compressed manner to begin with.

Consider a scenario where we are interested in recovering a vector $x \in \mathbb{R}^N$. We refer to the domain of vector x as the primal domain. For 2D signals, vector x can represent the columns of the matrix of interest stacked up to form

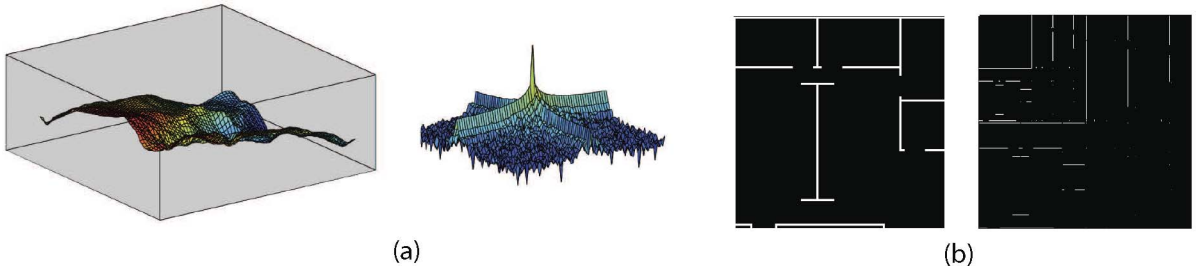

Fig. 2. (a, left) Height map of part of Sandia Mountains in New Mexico—courtesy of US Geological Survey [26], and (a, right) its transformed representation (Fourier) where more than 99.9999 percent of energy is in less than 3 percent of the coefficients. (b, left) An obstacle map with the obstacles denoted in white, and (b, right) its transformed representation (Haar wavelet) where 100 percent of energy is in less than 1 percent of the coefficients. For visual clarity, refer to the online pdf for the color version of this image.

a vector (a similar approach can be applied to higher order signals). Let $y \in \mathbb{R}^K$ where $K \ll N$ represent the incomplete linear measurement of vector x obtained by the sensors. We will have

$$y = \Phi x, \tag{1}$$

where we refer to Φ as the observation matrix. Clearly, solving for x based on the observation set y is an ill-posed problem as the system is severely under-determined ($K \ll N$). However, suppose that x has a sparse representation in another domain, i.e., it can be represented as a linear combination of a small set of vectors

$$x = \Gamma X, \tag{2}$$

where Γ is an invertible matrix and X is S-sparse, i.e., $|\mathrm{supp}(X)| = S \ll N$ where $\mathrm{supp}(X)$ refers to the set of indices of the nonzero elements of X and $|\cdot|$ denotes its cardinality. This means that the number of nonzero elements in X is considerably smaller than N. Then we will have

$$y = \Psi X, \tag{3}$$

where $\Psi = \Phi \times \Gamma$. We refer to the domain of X as the sparse domain (or transform domain). If $S \leq K$ and we knew the positions of the nonzero coefficients of X, we could solve this problem with traditional techniques like least-squares. In general, however, we do not know anything about the structure of X except for the fact that it is sparse (which we can validate by analyzing similar data). The new theory of compressive sensing allows us to solve this problem.

Theorem 1. *If $K \geq 2S$ and under specific conditions, the desired X is the solution to the following optimization problem:*

$$\min \|X\|_0, \text{ such that } y = \Psi X, \tag{4}$$

where $\|X\|_0 = |\mathrm{supp}(X)|$ represents the zero norm of vector X. (See [18] for details and the proof.)

Theorem 1 states that we only need $2 \times S$ measurements to recover X and therefore x fully. This theorem, however, requires solving a nonconvex combinatorial problem, which is not practical. For over a decade, mathematicians have worked toward developing an almost perfect approximation to the ℓ_0 optimization problem of Theorem 1 [27], [28]. Recently, such efforts resulted in several breakthroughs.

More specifically, consider the following ℓ_1 relaxation of the aforementioned ℓ_0 optimization problem:

$$\min \|X\|_1, \text{ subject to } y = \Psi X. \tag{5}$$

Theorem 2. *Assume that X is S-sparse. The ℓ_1 relaxation can exactly recover X from measurement y if matrix Ψ satisfies the Restricted Isometry Condition for $(2S, \sqrt{2}-1)$, as described below. (See [29], [18], [30], [31], [19] for details, the proof, and other variations.)*

Restricted Isometry Condition (RIC) [32]: Matrix Ψ satisfies the RIC with parameters (Z, ϵ) for $\epsilon \in (0,1)$ if

$$(1-\epsilon)\|c\|_2 \leq \|\Psi c\|_2 \leq (1+\epsilon)\|c\|_2, \tag{6}$$

for all Z-sparse vector c.

The RIC is mathematically related to the uncertainty principle of harmonic analysis [32]. However, it has a simple intuitive interpretation, i.e., it aims at making every set of Z columns of the matrix Ψ as orthogonal as possible. Other conditions and extensions of Theorem 2 have also been developed [33], [34]. While it is not possible to define all the classes of matrices Ψ that satisfy RIC, it is shown that random partial Fourier matrices [35] as well as random Gaussian [36], [37] or Bernoulli matrices [38] satisfy RIC (a stronger version) with the probability $1 - O(N^{-M})$ if

$$K \geq B_M S \times \log^{O(1)} N, \tag{7}$$

where B_M is a constant, M is an accuracy parameter and $\mathrm{O}(\cdot)$ is Big-O notation [18]. Equation 7 shows that the number of required measurements could be considerably less than N.

While the recovery of sparse signals is important, in practice signals may rarely be sparse. Many signals, however, are compressible. In practice, the observation vector y will also be corrupted by noise. The ℓ_1 relaxation and the corresponding required RIC condition can be easily extended to the case of noisy observations with compressible signals [29].

The possibility presented by the new theory of sampling, i.e., recovering signals from a considerably incomplete data set has sparked new research in different fields. A good example of a new resulting technology is the recent development of a compressive imaging camera that efficiently captures a single-pixel image, by producing a Ψ with Bernoulli distribution using pseudorandom binary patterns [39]. Other applications include medical imaging [40], DNA decoding [41], and computer graphics [42] among others.

3.1 Basis Pursuit: Reconstruction Using ℓ_1 Relaxation

The ℓ_1 optimization problem of (5) can be posed as a linear programming problem [43]. The compressive sensing algorithms that reconstruct the signal based on ℓ_1 optimization are typically referred to as "Basis Pursuit" [19]. Reconstruction through ℓ_1 optimization has the strongest known recovery guarantees [32]. However, the computational complexity of such approaches can be high. SPARSA [44], GPSR [45], and AC [46] are a few examples of the continuing attempts to reduce the computational complexity of the convex relaxation approach.

3.2 Matching Pursuit: Reconstruction Using Successive Interference Cancellation

The Restricted Isometry Condition implies that the columns of matrix Ψ should have a certain near-orthogonality property. Let $\Psi = [\Psi_1 \Psi_2 \cdots \Psi_N]$, where Ψ_i represents the ith column of matrix Ψ. We will have $y = \sum_{j=1}^{N} \Psi_j X_j$, where X_j is the jth component of vector X. Consider recovering X_i:

$$\frac{\Psi_i^H y}{\Psi_i^H \Psi_i} = \underbrace{X_i}_{\text{desired term}} + \underbrace{\sum_{j=1, j\neq i}^{N} \frac{\Psi_i^H \Psi_j}{\Psi_i^H \Psi_i} X_j}_{\text{interference}}. \tag{8}$$

If the columns of Ψ were orthogonal, then (8) would have resulted in the recovery of X_i. For an under-determined system, however, this will not be the case. Then, there are two factors affecting recovery quality based on (8). First, how orthogonal is the ith column to the rest of the columns and second how strong are the other components of X. In other words, it is desirable to first recover the strongest component of X, subtract its effect from y, recover the second strongest component and continue the process. Adopting the terminology of Code Division Multiple Access (CDMA) in communication literature, we refer to such approaches as *Successive Interference Cancellation*. In fact, if $X_i \neq 0$, one can think of Ψ_i coding X_i. If the ith code is used as in (8), then ideally X_j for $j \neq i$ cannot be decoded properly and only X_i can be recovered.

Such successive cancellation methods have been used in the context of CDMA systems in communication literature for recovering the signals of different users at the base station [47], [48]. While the context of the two problems may seem different, they share a very core fundamental form. Recently, Tropp and Gilbert independently proposed using a version of successive interference cancellation in the context of compressive sampling and derived the conditions under which it can result in an almost perfect recovery [25]. They refer to it as Orthogonal Matching Pursuit (OMP). Similar to Successive Interference Cancellation, the basic idea of OMP is to iteratively multiply the measurement vector, y, by Ψ^H, recover the strongest component, subtract its effect and continue again. Let I_{set} denote the set of indices of the nonzero coefficients of X that is estimated and updated in every iteration. Once the locations of the S nonzero components of X are found, we can solve directly for X by using a least squares solver:

$$\hat{X} = \underset{X\,:\,\text{supp}(X)=I_{\text{set}}}{\text{argmin}} \|y - \Psi X\|_2. \tag{9}$$

A variation of OMP, Regularized Orthogonal Matching Pursuit (ROMP), was later introduced by Needell and Vershynin [32]. The main difference in ROMP, as compared to OMP, is that in each iterative step, a set of indices (locations of vector X with nonnegligible components) are recovered at the same time instead of only one at a time, resulting in a faster recovery [32]. Other variations of this work (some under different names) have also appeared [32], [33], [34], [35], [36], [37], [38], [39], [40], [41], [42], [43], [44], [45], [46], [47], [48], [49]. Algorithm 1 shows a summary of the steps involved in Matching Pursuit approaches. Function Υ in the second step is $\Upsilon(y^{\text{new}}) = y^{\text{new}}$ for OMP and ROMP. Consequently, $\Psi_u = \Psi$ in the third step in this case. Then, X_{proj} represents the projection of the measurement y to the columns of matrix Ψ. This projection serves as the base for deciding the indices that correspond to the significant coefficients of X. Let x_{proj} represent the signal that corresponds to X_{proj} in the primal domain: $x_{\text{proj}} = \Gamma X_{\text{proj}}$. In applications where X represents the Fourier transformation of x, we have $\Gamma^{-1} = \Gamma^H$ (this is the case for several applications). Furthermore, for the cases where the signal was point sampled in the primal domain (we will see such cases in the next section), the measurement matrix Φ will have exactly one 1 in every row and at most one 1 at every column, with the rest of the elements zero. Therefore, we will have

$$x_{\text{proj}} = \Phi^H y, \tag{10}$$

where x_{proj} will be the same as y at the measured points but will be zero elsewhere. Although X_{proj} does not exactly serve as an estimate of X, it does serve as a base for deciding the index set. Therefore, it may not be a good starting point for some applications since it assumes that the signal is zero at unmeasured points in the primal domain. If x represents the spatial variations of an aerial map, for instance, having zero in between the acquired measurements is not a realistic initial estimate. In other words, both OMP and ROMP do not consider the progression of the reconstructed signal in the primal domain and only process the signal in the sparse domain. In order to address this, we proposed *Interpolated ROMP* (I-ROMP) [2], an extension of ROMP [32] which can provide a better performance for certain applications. In I-ROMP, we take advantage of processing the signal in both the primal domain (domain of x) as well as the sparse domain (domain of X). At every iteration, we start by up-sampling the residual vector y^{new} through interpolation

$$y_u^{\text{new}} = \Upsilon_{\text{interp}}(y^{\text{new}}), \Upsilon_{\text{interp}} : \mathbb{R}^K \rightarrow \mathbb{R}^N, \tag{11}$$

where function Υ_{interp} represents an up-sampling function such as an interpolator. Then, we have $\Upsilon = \Upsilon_{\text{interp}}$ in the second step, and Ψ_u is the full $N \times N$ version of Ψ matrix in the third step for I-ROMP. The rest of the steps remain the same. Throughout the paper, we discuss which approach is suitable for the considered application. It should be noted that the target sparsity of Algorithm 1 is typically set to a percentage of the number of measurements gathered [50].

Algorithm 1. A Summary of Matching Pursuit Approaches (OMP [25], ROMP [32], and I-ROMP [2])

Input: measured vector $y \in \mathbb{R}^K$, target sparsity S, and size of full signal N

Output: set of indices $I_{\text{set}} \subset \{1, \ldots, N\}$ of non-zero coefficients in X with $|I_{\text{set}}| \leq S$, and $\hat{X}$, the estimated X.

Initialize: $I_{\text{set}} = \emptyset$ and $y^{\text{new}} = y$

1: **while** stop criteria not met **do**
2: $y_u^{\text{new}} = \Upsilon(y^{\text{new}})$
3: $X_{\text{proj}} = \Psi_u^H y_u^{\text{new}}$
4: choose a subset of indices from X_{proj} based on a utilized criteria for deciding the significant coefficients
5: update index set I_{set}
6: $\hat{X} = \underset{X:\text{supp}(X)=I_{\text{set}}}{\text{argmin}} \|y - \Psi X\|_2$
7: $y^{\text{new}} = y - \Psi \hat{X}$
8: **end while**

While ℓ_1 relaxation of the previous part can solve the compressive sampling problem with performance guarantees, the computational complexity of the iterative greedy approaches of this part can be considerably less [25]. In the next section, we use both approaches when reconstructing the signal.

4 Compressive Cooperative Mapping in Mobile Networks

In this section, we show how the new theory of compressive sampling and reconstruction can result in the efficient mapping of a spatial function in mobile cooperative networks. In particular, we discuss three main areas, cooperative aerial mapping, mapping of the obstacles, and mapping of the communication signal strength.

There are three main factors affecting how well a sampled function can be reconstructed using the compressive sampling framework: 1) the domain in which it was sampled, 2) its sparsity in a targeted transform domain, and 3) the RIC of the resulting Ψ matrix (see Table 1). As an example, consider an obstacle map where nonzero values represent obstacles. An obstacle map is typically sparse in the spatial domain, i.e., it has localized features. As a result in the Fourier domain, it is not very compressible. Therefore, point sampling it in the spatial domain and using sparsity in the Fourier domain will not result in an efficient reconstruction. An obstacle map is also sparse in the wavelet domain. However, the Ψ matrix that results from point sampling in the spatial domain and using wavelet transform will not meet the RIC condition, making this approach unsuitable. Therefore, in order to have a compressive and efficient reconstruction of an obstacle map, one should consider other possibilities for sensing and reconstruction, as we shall propose in this section. For spatial functions that are not sparse in the spatial domain, such as an aerial map, applying Fourier transformation can result in a considerably compressible function. As discussed earlier, it has been proved that the Ψ matrix that results from point sampling in the spatial domain and using Fourier transform for reconstruction also meets the RIC condition, making it suitable for compressive reconstruction. In the rest of the section, we first consider cooperative aerial mapping. We then proceed with compressive obstacle mapping and mapping of the communication signal strength.

4.1 Compressive Mapping of a Spatial Field of Interest: Cooperative Aerial Mapping

Consider a case where a group of Unmanned Air Vehicles are tasked with building an aerial map of a region, as shown in Fig. 1.[1] Then, x of (1) represents the aerial map of interest in the spatial domain, where the columns of the aerial map matrix are stacked up to form a vector. The vehicles make measurements in the spatial domain, i.e., vector y consists of the few measurements made by the vehicles. There is no requirement on a specific sampling pattern for the measurements. As such, the measurements could be gathered randomly. The Fourier transform of a height map can be considerably sparse, as is shown in Fig. 2a. Then, Fourier transformation can be used for sparse representation and reconstruction. Matrix Γ represents the inverse Fourier transformation matrix and matrix Φ will be as follows:

1. The approach of this section is equivalently relevant if there is only one UAV that is gathering the measurements over time.

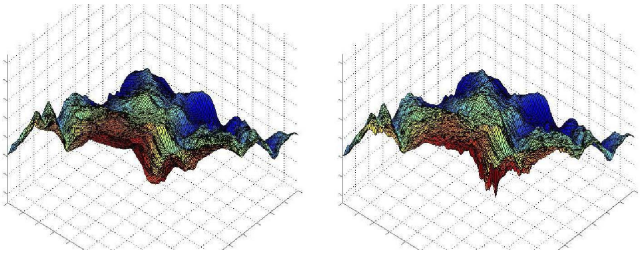

Fig. 3. Demonstration of the reconstruction of a height map (as applicable to UAV applications) with only 30 percent measurements using compressive sensing. (left) The original height map of a portion of Albuquerque Sandia Mountains (courtesy of US Geological Survey [26]). (right) Reconstruction using compressive mapping with only 30 percent random measurements. The normalized MSE of the reconstruction is 7.5×10^{-8}. For visual clarity, refer to the online pdf for the color version of this image.

$$\begin{aligned}&\forall i\ 1 \le i \le K, \exists j\ 1 \le j \le N \text{ such that } \Phi(i,j) = 1 \text{ and}\\ &\forall i\ 1 \le i \le K, \forall j \ne j', 1 \le j, j' \le N, \text{ if } \Phi(i,j) = 1 \rightarrow \Phi(i,j') = 0,\end{aligned} \tag{12}$$

where it represents a matrix with only one 1 in every row. If there are redundant measurements, they may be more than one 1 in every column. Otherwise, there will be at most one 1 in every column. This matrix is the result of point sampling in the spatial domain. Fig. 3 (left) shows an aerial map of a portion of the Sandia Mountains in Albuquerque, NM. Then, vector x represents the height values of the mountain range, stacked up to form a vector. Fig. 3 (right) shows our reconstruction when only 30 percent of the area is sensed. We used I-ROMP of Algorithm 1 for reconstruction and exploited the sparse representation of the signal in the Fourier domain. The normalized Mean Square Error (MSE) of this reconstruction is 7.5×10^{-8}. It can be seen that the reconstructed map is almost identical to the real map. In this figure, the measurement points are randomly distributed over the area of interest. In practice, it would be hard for a number of mobile units (or one) to randomly point sample the area. For instance, a number of UAVs would make measurements along their trajectories. Therefore, we next show the performance when measurements are gathered randomly over line trajectories or Brownian motions. Fig. 4 shows compressive reconstruction of a smaller part of the Sandia height map, with only 10.33 percent measurements. The middle figure of the top row, shows the reconstruction when the measurements are randomly distributed over the area of interest, for the original map shown in the left figure. The right figure, on the other hand, shows the case where the same number of measurements is gathered over random line trajectories. Fig. 5 (left) shows an example of the random line trajectories, which were used for the reconstruction of Fig. 4 (right). It can be seen that using random line measurements (instead of random point samples) results in a loss of performance as the normalized MSE increases from 4×10^{-7} (for the middle top row figure) to 5.9×10^{-6} (for the right figure). This is expected as the derivations and performance guarantees of compressive sampling theory are based on purely random samples. Still, the MSE is considerably low for both cases and they provide useful information about the field of interest with very few measurements. In this case, we used I-ROMP for the

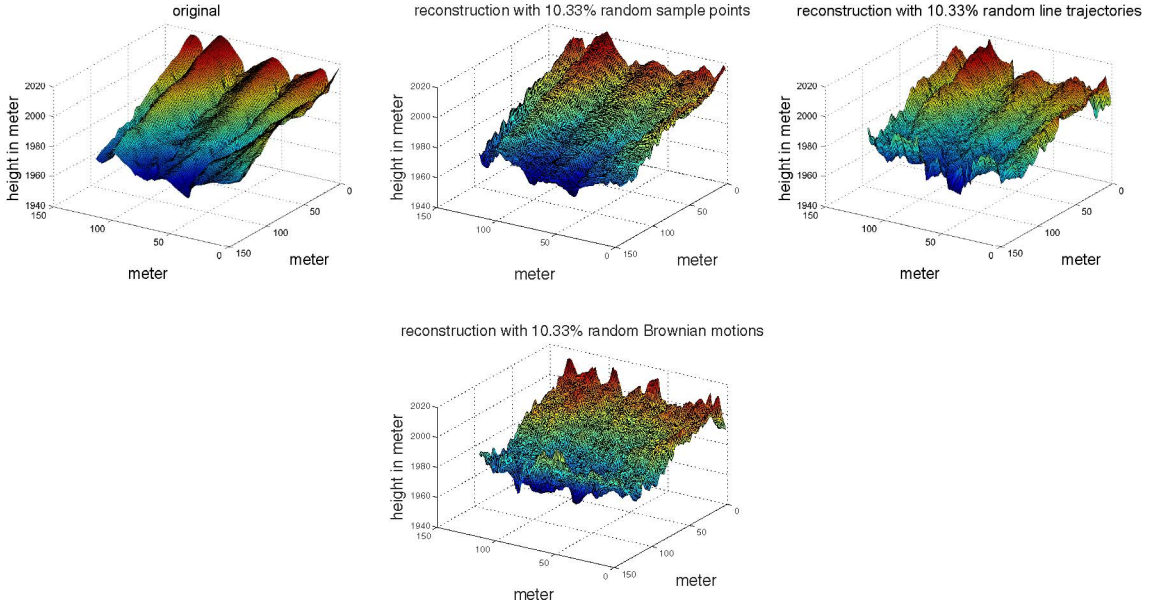

Fig. 4. Demonstration of compressive reconstruction of part of the height map of Albuquerque Sandia Mountains with only 10.33 percent measurement: (left) the original map from [26], (middle top row) reconstruction using random point samples with normalized MSE of 4×10^{-7}, (right) reconstruction using random line trajectories of Fig. 5 (left) with normalized MSE of 5.9×10^{-6}, and (bottom) reconstruction using random Brownian motion trajectories of Fig. 5 (right) with normalized MSE of 1.186×10^{-5}. For visual clarity, refer to the online pdf for the color version of this image.

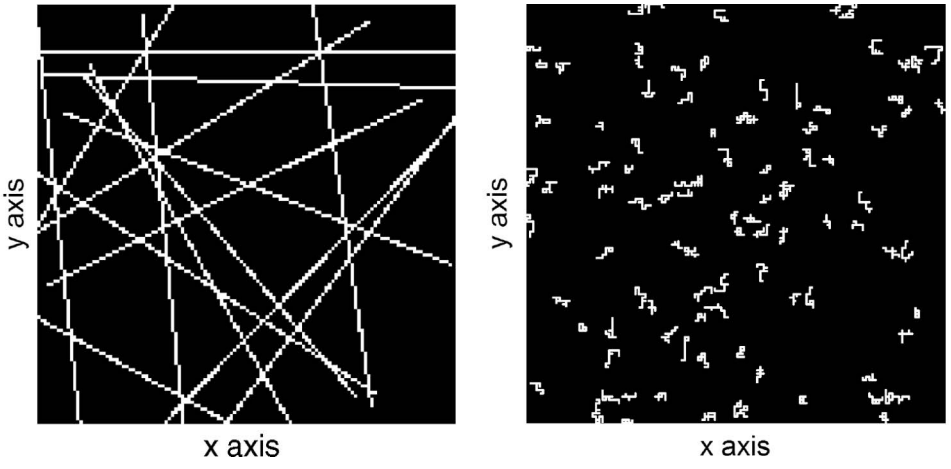

Fig. 5. (left) Random line trajectories of UAVs used in the reconstruction of Fig. 4 (middle top row) and (right) Random Brownian motion trajectories of UAVs used in the reconstruction of Fig. 4 (bottom).

reconstruction of the middle figure. However, when the samples are more localized as is the case for the right figure, I-ROMP's performance degrades. This is due to the fact that I-ROMP combines spatial interpolation with compressive sensing. Therefore, as the sampling positions become more clustered, its performance degrades. We then used an ℓ_1 relaxation approach for the reconstruction of the right figure. OMP also provides a similar result with a slightly higher MSE. Finally, Fig. 4 (bottom) shows the reconstruction quality when a swarm of UAVS have random Brownian motions, as shown in Fig. 5 (right). While the overall percentage of measurements of this case is still 10.33 percent, some of the points may be revisited due to the utilized Brownian motions, which can reduce the number of overall useful measurements. Furthermore, the measurements are more clustered in this case, which can further degrade the performance. We therefore used an ℓ_1 relaxation approach for this reconstruction, which results in the normalized MSE of 1.186×10^{-5}. As can be seen, the normalized MSE is not as low as the previous two cases but can still be low enough for several cooperative applications. Overall, the results indicate the potentials of compressive mapping framework for efficient sensing and reconstruction in mobile networks.

4.2 Compressive Cooperative Mapping of Obstacles

In this section, we show how a group of mobile nodes can build a high-quality map of the obstacles with minimal sensing and without directly sampling a high percentage of the area. Accurate mapping of the obstacles is considerably important for the robust operation of a mobile network. Yet the high volume of the information presented by the environment makes it prohibitive to sense all the areas, making accurate mapping considerably challenging. In this part, we show how the nodes can cooperatively build a map of the obstacles based on a considerably small set of observations. More specifically, we propose a *noninvasive*

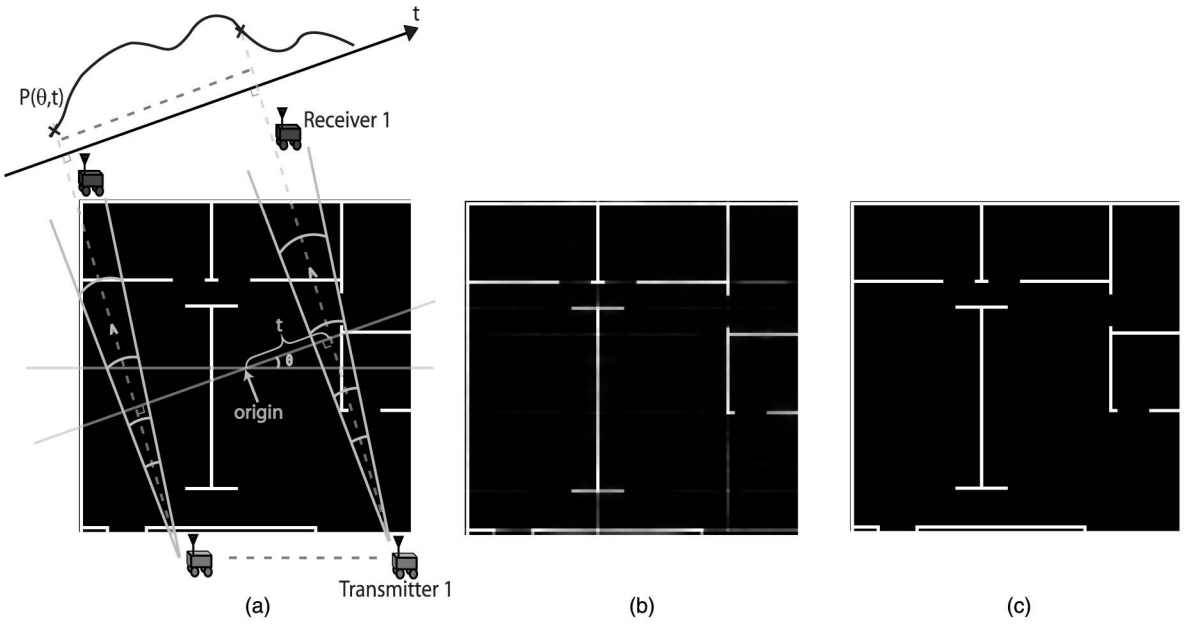

Fig. 6. (left) An indoor obstacle map with the obstacles marked in white and the illustration of the proposed compressive noninvasive mapping, (middle) Reconstruction of the map using the proposed framework with only 4 percent measurements, (right) Reconstruction of the map using the proposed framework with only 11.7 percent measurements—only shadowing and path loss are simulated. See the online pdf for a better visual clarity.

mapping strategy, which is enabled by the theory of compressive sampling. By noninvasive mapping, we refer to a mapping technique that allows the vehicles to map the obstacles without sensing them directly. For instance it allows the robots to map the obstacles inside a building or a room before entering it. To the best of author's knowledge, there is currently no framework for efficient noninvasive mapping of obstacles.

As was discussed earlier, a map of obstacles is sparse in the spatial or wavelet domain, which makes point sampling in the spatial domain unsuitable for reconstruction, using the compressive mapping framework. In this section, we propose a new sensing method for mapping of obstacles, which is noninvasive and only uses wireless channel measurements.

4.2.1 Compressive Noninvasive Mapping of Obstacles: A New Possibility for Noninvasive Mapping

In this part, we propose a new noninvasive technique for mapping of the obstacles. In general, devising noninvasive mapping strategies can be considerably challenging. Motivated by computed tomography approaches to medical imaging [51], geology [52], and computer graphics [53], we show how our proposed compressive mapping framework can result in a new and efficient *noninvasive sensing* technique for mapping obstacles, based on wireless channel measurements. Consider the case where a number of vehicles want to build a map of the obstacles inside a building before entering it. *Noninvasive mapping allows the nodes to assess the situation before entering the building and can be of particular interest in several applications such as an emergency response.* In this part, we consider building a 2D map (our proposed approach can be extended to 3D maps as well). Fig. 6 (left) shows a sample 2D map where a number of vehicles want to map the space before entering it. Let $g(u,v)$ represent the binary map of the obstacles at position (u,v) for $u,v \in \mathbb{R}$. We will have

$$g(u,v) = \begin{cases} 1, & \text{if } (u,v) \text{ is an obstacle,} \\ 0, & \text{else.} \end{cases} \tag{13}$$

Consider communication from Transmitter 1 to Receiver 1, as marked in Fig. 6 (left). A fundamental parameter that characterizes the performance of a communication channel is the received signal power, which is measured at every receiver [54]. There are three time-scales associated with the spatio-temporal changes of the channel quality and therefore received signal strength [55], as indicated in Fig. 7. The slowest dynamic is associated with the signal attenuation due to the distance-dependent power fall-off (path loss). Then there is a faster variation referred to as shadow fading (shadowing), which is due to the impact of the blocking objects. This means that each obstacle along the transmission path leaves its mark on the received signal by

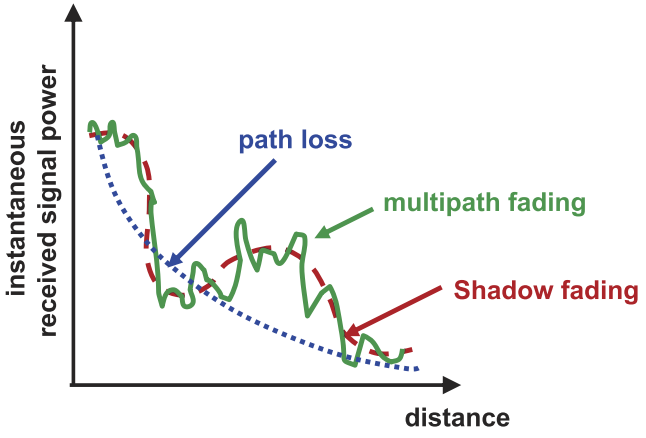

Fig. 7. A multiscale representation of the received signal power in a wireless transmission [54].

attenuating it to a certain degree characterized by its properties. Finally, depending on the receiver antenna angle, multiple replicas of the transmitted signal can arrive at the receiver due to the reflection from the surrounding objects, resulting in multipath fading, a faster variation in the received signal power [56].

A communication from Transmitter 1 to Receiver 1 in Fig. 6 (left), therefore, contains implicit information of the obstacles along the communication path. Consider the dashed ray (line) that corresponds to distance t and angle θ in Fig. 6 (left). This line is at distance t from the origin and is perpendicular to the line that is at angle θ with the x-axis. Let $P(\theta,t)$ represent the received signal power in the transmission along the ray that corresponds to distance t and angle θ, as shown in Fig. 6 (left). We will have [55], [56]

$$P(\theta,t) = P_s(\theta,t)w(\theta,t), \tag{14}$$

where

$$P_s(\theta,t) = \underbrace{\frac{\beta P_T}{\big(d(\theta,t)\big)^{\alpha}}}_{\text{path loss}} \times \underbrace{e^{\sum_i r_i(\theta,t)n_i(\theta,t)}}_{\text{shadowing due to obstacles}}, \tag{15}$$

represents the contribution of distance-dependent path loss and shadowing. For the path loss term, P_T represents the transmitted power, $d(\theta,t)$ is the distance between the transmitter and receiver across that ray, α is the degradation exponent, and β is a constant that is a function of system parameters. For the shadowing (or shadow fading) term, r_i is the distance traveled across the ith object along the (θ,t) ray and $n_i < 0$ is the decay rate of the wireless signal within the ith object. Furthermore, the summation is over the objects across that line. As can be seen, shadowing characterizes wireless signal attenuation as it goes through the obstacles along the transmission path and therefore contains information about the objects along that line.

$w(\theta,t)$ of (14), on the other hand, is a positive random variable with unit average, which models the impact of multipath fading. There are a number of well-established models for the distribution of $w(\theta,t)$ in the communication literature [54]. Nakagami power distribution or its special cases such as Rician power or exponential are common models.[2] For more mathematical details on wireless channel modeling, readers are referred to [54], [55], [56]. We can then model $\ln P(\theta,t)$ as follows:

$$\ln P(\theta,t) = \underbrace{\ln P_T}_{\text{transmitted power in dB}} + \underbrace{\beta_{\text{dB}} - \alpha \ln d(\theta,t)}_{\text{path loss } (\le 0)} + \underbrace{\sum_i r_i(\theta,t)n_i(\theta,t)}_{\text{shadowing effect due to blocking objects } (\le 0)} + \underbrace{w_{\text{dB}}(\theta,t)}_{\text{multipath fading}}, \tag{16}$$

where $\beta_{\text{dB}} = \ln\beta$ and $w_{\text{dB}} = \ln w(\theta,t)$. Then, we have

$$\begin{aligned} h(\theta,t) &\triangleq \ln P(\theta,t) - \ln P_T - \big(\beta_{\text{dB}} - \alpha \ln d(\theta,t)\big) \\ &= \underbrace{\sum_i r_i(\theta,t)n_i(\theta,t)}_{\text{shadow fading effect}} + \underbrace{w_{\text{dB}}(\theta,t)}_{\text{multipath fading}}. \end{aligned} \tag{17}$$

Path loss and shadowing represent the signal degradation due to the distance traveled and obstacles, respectively, and $w_{\text{dB}}(\theta,t)$ represents the impact of multipath fading. By using an integration over the line that corresponds to θ and t, we can express (17) as follows:

$$h(\theta,t) = \int\int_{\text{line}(\theta,t)} g_n(u,v)\,du\,dv + w_{\text{dB}}(\theta,t), \tag{18}$$

where

$$g_n(u,v) = \begin{cases} n(u,v), & \text{if } g(u,v) = 1, \\ 0, & \text{else}, \end{cases} \tag{19}$$

with $g(u,v)$ representing the binary map of the obstacles (indicated by (13)) and $n(u,v)$ denoting the decay rate of the signal inside the object at position (u,v) (see $n_i(\theta,t)$ in (15)). $g_n(u,v)$ then denotes the true map of the obstacles, including wireless decay rate information. By changing t at a specific θ, a projection is formed, i.e., a set of ray integrals, as is shown in Fig. 6 (left). Let $G_n(\theta_f,f)$ represent the 2D Fourier transform of g_n expressed in the polar coordinates. Let $H_t(\theta,f)$ denote the 1D Fourier transform of $h(\theta,t)$ with respect to t: $H_t(\theta,f) = \int h(\theta,t)e^{-j2\pi ft}dt$. We have the following theorem.

Fourier Slice Theorem [51]: Consider the case where there is no multipath fading in (18), i.e., $w_{\text{dB}} = 0$. Then $H_t(\theta,f)$, the Fourier transformation of $h(\theta,t)$ with respect to t, is equal to the samples of $G_n(\theta_f,f)$ across angle $\theta_f = \theta$.

Consider the illustrated line at angle θ that passes through the origin in Fig. 6 (left). Two robots can move outside the room such that the straight line between them is perpendicular to the illustrated line at angle θ. Then the receiving robot measures $P(\theta,t)$, the received signal power at different ts. In practice, the parameters of the path loss component of the received signal in (16) can be estimated by using a few Line Of Sight (LOS) transmissions in the same environment. Therefore, the impact of path loss can be removed and the receiving robot can calculate $h(\theta,t)$. By making a number of measurements at different ts for a given θ, the Fourier Slice Theorem allows us to measure the samples of the Fourier transform of the map g_n at angle θ. By changing θ, we can sample the Fourier transform of the map of the obstacles at different angles. We can then pose the problem in a compressive sampling framework. By measuring the received signal power across the rays, the vehicles can indirectly sample the Fourier transformation of the obstacle map. Then the sparsity in the spatial or wavelet domain could be used for reconstruction.

Let x of (1) denote the vector representation of G_n (2D Fourier transform of the obstacle map), where the columns of G_n are stacked up to form a vector. Then y represents the very few samples of G_n acquired using the proposed framework, i.e., wireless channel measurements across a number of rays and the Fourier Slice Theorem. By utilizing the sparse representation of the map in the spatial or

2. Rician is a possible distribution for $\sqrt{w(\theta,t)}$. Thus we use the term "Rician power" to indicate that we are referring to the corresponding distribution for $w(\theta,t)$.

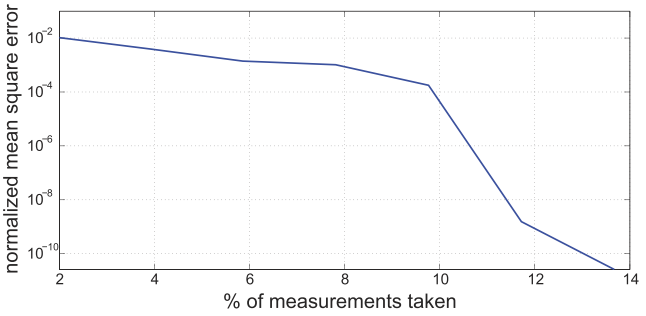

Fig. 8. Normalized Mean Square Error for the reconstruction of the map of Fig. 6 (left) as a function of the percent of measurements taken—only shadowing and path loss are simulated.

wavelet domain, the vehicles can solve for the map cooperatively, based on minimal measurements, and more importantly in a noninvasive manner. For reconstruction based on sparsity in the spatial domain, X will be the vector representation of g_n, Φ is as denoted in (12) and Γ is the Fourier transform matrix. Then, the Ψ matrix that results from point sampling in the frequency domain and reconstruction using sparsity in the spatial domain will meet the RIC condition [35]. Since the changes in the map are typically sparser than the map itself, another approach is to consider and minimize the variations in X. This approach is referred to as Total Variation (TV) [18]. Typically, an obstacle map is also considerably sparse in the wavelet domain (as shown in Fig. 2b). Let X represent the vector representation of the wavelet transform of the obstacle map. Then, $\Gamma = F \times W^{-1}$ and Φ is as described earlier. In this formulation, F and W represent the 2D Fourier and wavelet matrices such that when applied to a vector that is formed by stacking the columns of a 2D map, they result in the vector representation of the 2D Fourier and wavelet transform of the map, respectively.

Fig. 6 (middle and right) shows our results for noninvasive compressive mapping of the obstacles of the left figure. For this result, no multipath fading is simulated. We will discuss and show the impact of multipath fading in the next part. For this figure, our reconstruction is based on minimizing Total Variation, using ℓ_1 magic toolbox [57]. It can be seen that with only 11.7 percent measurements (right figure), the map can be built almost perfectly. Note that 11.7 percent measurements implies that 11.7 percent of the 2D Fourier transformation of the map is only sampled. Even with 4 percent measurements (middle figure), the reconstruction is very close to the original. Fig. 8 shows the normalized MSE of the reconstruction of the obstacle map of Fig. 6 (left) as a function of the percentage of the measurements taken. It can be seen that a cooperative network can build a high-quality and noninvasive map of obstacles with a considerably small set of measurements.

Next, we compare the performance with interpolation approaches [15]. Fig. 9 (left) shows the performance of our proposed compressive reconstruction approach (under the same condition as Fig. 6 (right)). Fig. 9 (right) shows the reconstruction using interpolation on the acquired frequency samples, for the case where 11.7 percent wireless measurements are gathered and in the absence of multipath fading. As can be seen, the performance degrades considerably for the right figure as interpolation-based approaches are not suitable for reconstructing obstacle maps.

4.2.2 Impact of Multipath Fading

So far we proposed a compressive mapping framework for noninvasive mapping of the obstacles. In this part, we discuss the impact of multipath fading component of (14) on the proposed noninvasive reconstruction. Multipath fading can result in some noise in the observations, as can be seen from (18). We next add multipath fading, with a Rician distribution, to each wireless reception in a simulation environment. Rician fading is the most commonly considered distribution for multipath fading. This means that $w_{\text{sr}} = \sqrt{w(\theta, t)}$ has the following distribution (see (14)):

$$p(w_{\text{sr}}) = \frac{w_{\text{sr}}}{\sigma^2} \exp\left(\frac{-(w_{\text{sr}}^2 + \nu^2)}{2\sigma^2}\right) I_0\left(\frac{w_{\text{sr}}\nu}{\sigma^2}\right), \tag{20}$$

where $I_0(.)$ is the zeroth-order modified Bessel function of the first kind, ν^2 is the power of the Line Of Sight component and $2\sigma^2$ is the power of the multipath terms. We then define the following parameter to measure the strength of the LOS component, as compared to the total power: $\rho = \frac{\nu^2}{2\sigma^2 + \nu^2}$.

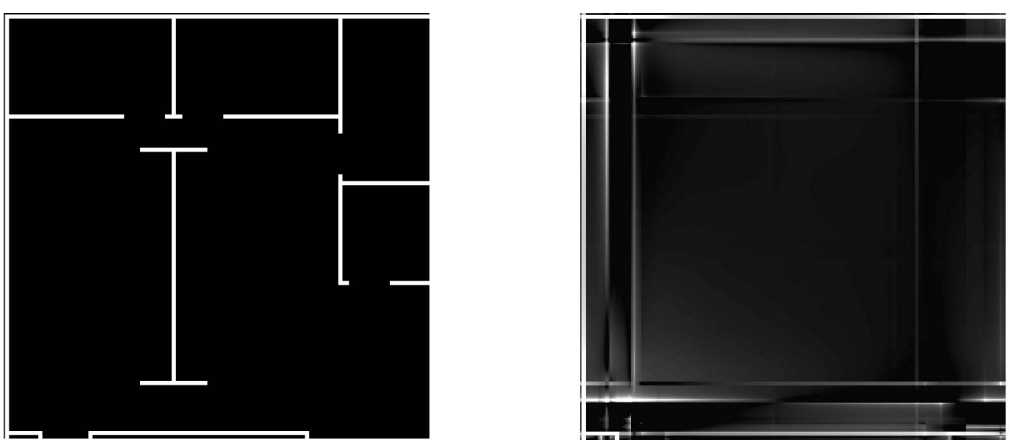

Fig. 9. Reconstruction of the map of Fig. 6 (left) with (left) our proposed approach and (right) interpolation. 11.7 percent measurements are used for both cases and no multipath fading is simulated. It can be seen that interpolation results in a considerable performance degradation.

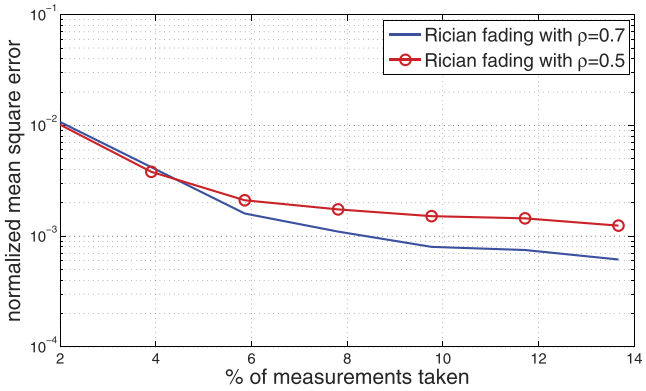

Fig. 10. Simulation of the impact of multipath Rician fading on the reconstruction of the map of Fig. 6 (left). Performance as a function of the percent measurements taken.

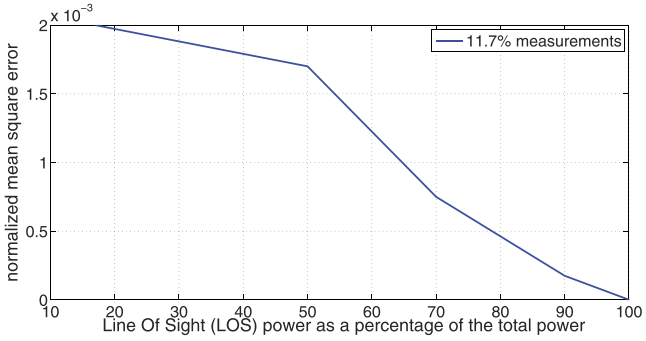

Fig. 11. Simulation of the impact of multipath Rician fading on the reconstruction of the map of Fig. 6 (left). Performance as a function of ρ.

Fig. 10 shows the normalized MSE of reconstruction in the presence of Rician multipath fading, with $\rho = 0.5$ and $\rho = 0.7$, while Fig. 11 shows the performance as a function of ρ, for the case where 11.7 percent measurements were taken. $\rho = 0.5$, for instance, indicates that half of the received power is from multipath as opposed to the LOS component. As compared to the reconstruction performance in Fig. 8, where only shadow fading and path loss were considered, it can be seen that multipath fading results in some performance loss.

4.2.3 Further Extensions

We should note that the aforementioned modeling of a wireless channel cannot possibly embrace all the propagation phenomena. Thus, further experimental validations are needed. Still, the results of this section are very promising. In practice, the effect of multipath fading can also be reduced by using directional antennas as well as averaging the received signal over a very small distance. Designing a proper robotic experimental setup to show the performance of the proposed method in practice, however, is the subject of another paper of ours [58]. Thus, we next show one sample reconstruction of a real obstacle in order to merely show that our proposed approach works in practice. Readers are referred to [58] for more details.

Fig. 12 shows the performance of the proposed frequency sampling approach of this section in reconstructing a T-shaped obstacle on our campus, using only wireless measurements. The left figure shows a horizontal cut of the structure (which is what our approach reconstructs) while the right figure shows our reconstruction with only 9.09 percent measurements. As can be seen, the obstacle with all its details can be clearly seen.

4.3 Compressive Cooperative Mapping of Communication Signal Strength

In this section, we show how a group of mobile nodes can build a high-quality map of the communication signal strength cooperatively and with minimal sensing. Building a map of the communication signal strength is considerably important for the robust operation of several emerging networked robotics and control applications. In order to maintain connectivity, mobile nodes need to have an estimation of the communication signal strength in locations they have not yet visited. Currently, there is no framework for mapping of the communication signal strength with very few measurements. In this section, we show how the proposed compressive mapping framework can be utilized to estimate the spatial variations of the communication signal strength with very few observations. Our analysis of the spatial variations of several channel measurements has shown that a wireless channel can be considerably compressible in the Fourier domain. For

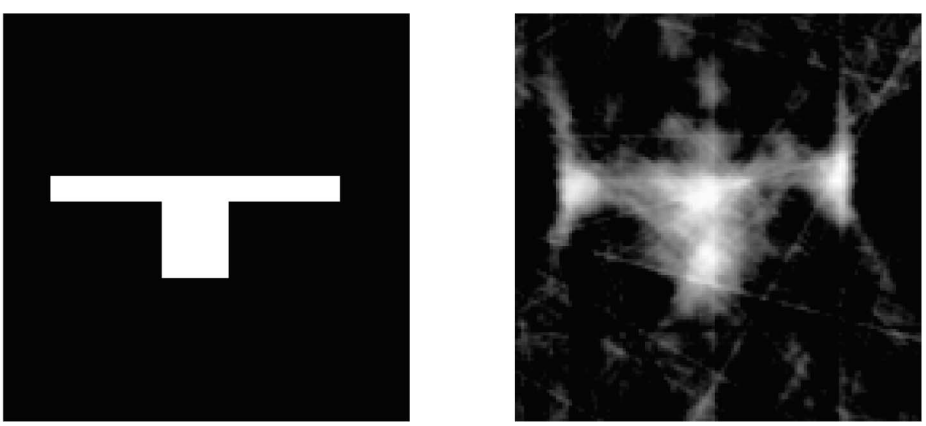

Fig. 12. Reconstruction of a T-shaped column on our campus. The left figure shows a horizontal cut of the column. The right figure shows our reconstruction of it, using the proposed frequency sampling approach, with 2 robots cooperatively making a very small number of wireless measurements (9.09 percent measurements).

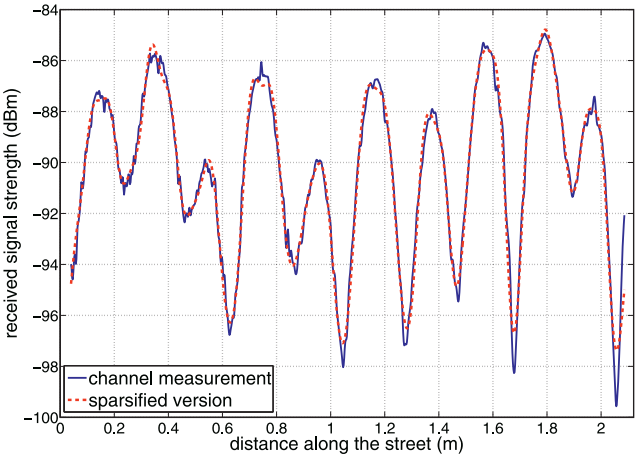

Fig. 13. Channel measurement along a street in San Francisco (courtesy of Mark Smith [60]) and its sparsified version. 99.99 percent of the energy of the measured channel is in 4.6 percent of its Fourier coefficients. As such, the two curves are almost identical.

instance, the solid line of Fig. 13 shows the measurement of a channel along a street in San Francisco [60]. For this channel, 99.99 percent of its energy is in 4.6 percent of its Fourier coefficients. The dashed line shows the sparsified version of the channel, where only the strongest 4.6 percent of the Fourier coefficients are kept. The two curves are almost identical and thus the spatial variations of the channel are compressible, i.e., a small percentage of the Fourier coefficients suffice for capturing the signal. Then, x of (1) represents the spatial map of the channel (received signal power). The vehicles make measurements in the spatial domain, i.e., vector y consists of the few measurements made by the vehicles. Consequently, matrix Φ will be as denoted in (12) and Γ is the inverse Fourier matrix.

4.3.1 Reconstruction of a Sparsified Channel

Equation (7) shows that for a sparse signal, if the number of measurements is above a certain level, the reconstruction can be perfect. In order to see this and get more insight into compressive sensing, we first consider reconstructing the sparsified version of the channel. As noted earlier, a wireless channel is compressible in the Fourier domain but not sparse. Therefore, our goal for reconstructing the sparsified version is to merely show the implication of (7). We will then proceed with reconstructing the channel itself.

The circle line of Fig. 14 shows the result of reconstructing the sparsified version of the signal of Fig. 13 based on a varying number of random observations, K. It should be noted that the channel measurements of Fig. 13 naturally contain the measurement noise. The size of the signal of Fig. 13 is $N = 1{,}024$. Fig. 14 then shows the average of the normalized Mean Square Error, averaged over 1,000 iterations with random samples, as a function of the number of measurements (K). The reconstruction method used for this figure is OMP. It can be seen that after a certain number of measurements are collected ($K = 270$ or 26 percent in this case), the construction becomes perfect (or bounded by computational errors) as predicted by (7).

Fig. 15 shows another real-world channel measurement in San Francisco, over a longer distance, along with its sparsified version. Due to the longer distance, this channel exhibits more nonstationary behavior, as can be seen. The length of the channel is $N = 4{,}096$ in this case. Our Fourier analysis showed that more than 99.995 percent of the energy of this measured signal is in less than 2.5 percent of its Fourier coefficients. Then the dashed line shows the sparsified version of the channel, where only the strongest 2.5 percent of the Fourier coefficients are kept. The dashed line of Fig. 14 shows the performance of compressive mapping in reconstructing the sparsified version of this channel. While the size of this signal is 4 times that of Fig. 13, the number of required observations (K) for perfect recovery is less than 2 times, as can be seen from Fig. 14. Overall, it can be seen that the compressive sensing approach can reconstruct the signal with a small number of measurements.

4.3.2 Reconstruction of Nonsparsified Channels

The previous section showed the strength of compressive sensing in reconstructing the spatial variations of the channel based on a considerably small measurement set. However, we showed the results for the sparsified version of the channel where it was possible to represent the signal

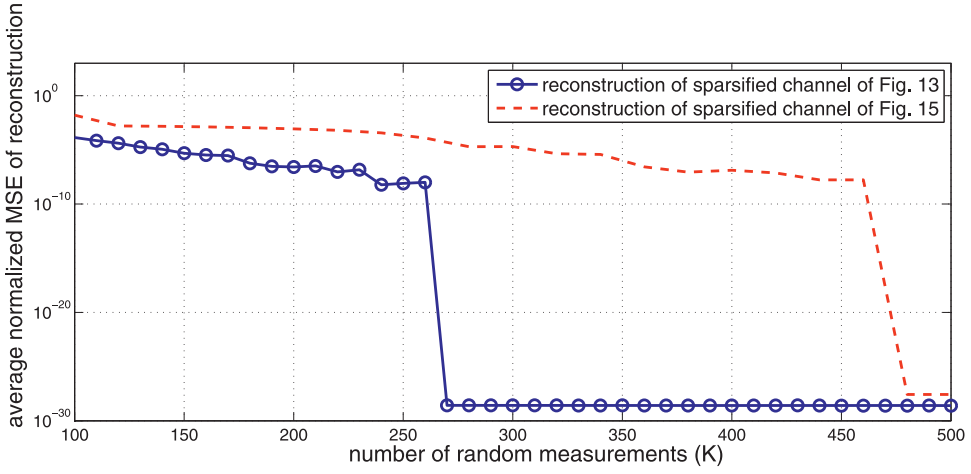

Fig. 14. Reconstruction of the sparsified signal of Figs. 13 and 15, based on an incomplete observation set, using compressive sensing. Length of x is $N = 1{,}024$ for the circle line and $N = 4{,}096$ for the dashed line.

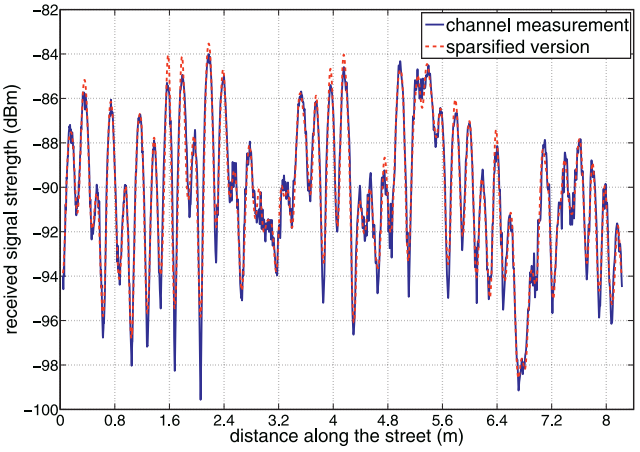

Fig. 15. Another channel measurement along a street in San Francisco (courtesy of Mark Smith [60]) and its sparsified version. The two curves are almost identical.

with only a small number of Fourier coefficients (the rest of the coefficients were zero as opposed to negligible). Fig. 16 shows the reconstruction of the measured channels of Figs. 13 and 15. It can be seen that the normalized MSE of both cases is considerably low. However, the error cannot be as low as that of Fig. 14, due to the fact that the signal is compressible but not sparse.

As expected, the channel of Fig. 15 has a higher MSE for the same number of measurements due to its longer length. We used OMP for these reconstructions. Based on our experience, ROMP's performance is considerably worse than OMP and I-ROMP. Depending on the sampling positions, I-ROMP could possibly perform better than OMP. For instance, if the samples are purely random (as was the case in this part), I-ROMP performs slightly better than OMP. On the other hand, for the cases where the samples are along line trajectories, as was discussed in Section 4.1 (see Figs. 4 and 5), I-ROMP's performance degrades and OMP or Basis Pursuit-type approaches should be used. Another example is the case where the samples are mainly distributed in a part of the channel with no samples in other parts. For instance, if all the samples are in the first half of the channel with no samples in the rest of the signal, OMP performs considerably better than I-ROMP. Overall, our results show that the proposed compressive mapping framework can build the spatial variations of the channel based on a considerably incomplete observation set. Furthermore, similar to the results in Section 4.1, reconstruction of a 2D channel, using line trajectories, can be achieved in a similar manner.

So far, we have shown the performance of the proposed sparsity-based approach in reconstructing two outdoor channels. We have seen similar results for other outdoor channels. We do, however, note that the compressibility of the channel can be different from area to area. More specifically, if an area is dominated by multipath fading, then channel compressibility can be less. In order to understand this better, we have made indoor measurements in the basement of the ECE building. This indoor environment is such that the channel experiences considerable amount of multipath fading. Thus, we can study how much we can still benefit from channel compressibility in the frequency domain for our proposed sparsity-based prediction. Fig. 17 (left) shows a 2D color map of the received signal strength in the area of interest. Fig. 17 (right) shows channel prediction performance in this area. As compared to Fig. 16, it can be seen that the prediction error is higher in this case, as expected. However, it can still be low enough for several applications.

Next, we compare the performance of the proposed sparsity-based channel prediction approach to that of model-based approaches. Recently, a number of papers have used underlying models for the field of interest, such as field average and correlation function, in order to estimate the spatial variations of a random field [16], [17], [61], [62]. In [61], [62], we developed a model-based approach for specifically predicting the spatial variations of a wireless channel, by using a multiscale dynamical model for the field. Consider the spatial variations of a wireless channel. From wireless communication literature, we know that we can represent the channel with three dynamics of path loss, lognormal shadowing and multipath fading (see Fig. 7). We then developed a prediction framework by taking the channel to be Gaussian (in dB), with an exponential correlation function, and with path loss

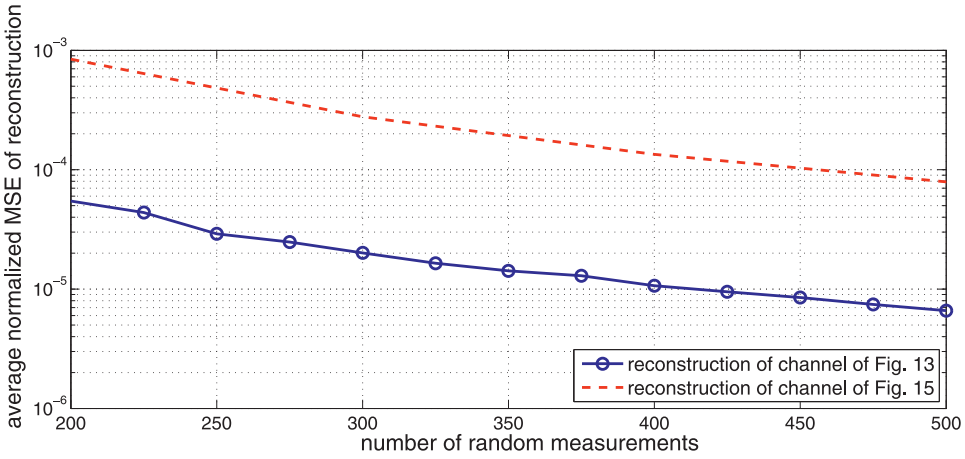

Fig. 16. Reconstruction of the measured channels of Figs. 13 and 15, based on an incomplete observation set, using compressive sensing. Length of x is $N = 1{,}024$ for the circle line and $N = 4{,}096$ for the dashed line.

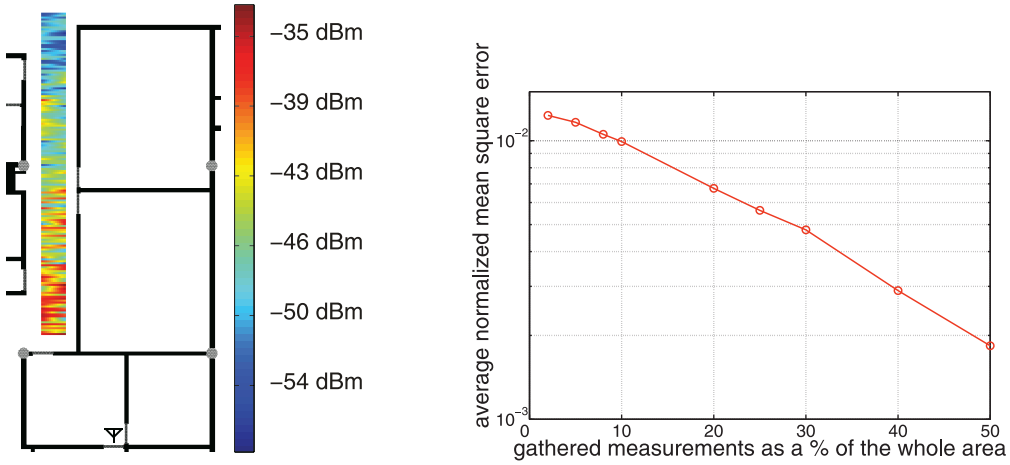

Fig. 17. (left) Indoor channel measurements, to the marked antenna, in the basement of ECE building (see the online pdf for a color version) and (right) its prediction quality as a function of the percent of measurements taken. As compared to Fig. 16 for outdoor channels, the error has increased due to an increase in multipath fading.

as its average. The main bottleneck of the model-based approach, as compared to the sparsity-based one, is estimating the underlying model parameters. As such, at very low sampling rates, the error in model discovery can be high, which propagates to channel prediction. Furthermore, in some environments, the underlying model parameters can change over a short distance, which can make the model discovery challenging. In such cases, the sparsity-based approach can outperform the model-based one. On the other hand, if the model can be estimated with a good enough accuracy, then the model-based approach can outperform the sparsity-based one, depending on the environment and the number of available a priori channel samples. In terms of computation, the model-based approach can have a high computational complexity, mainly due to the need for estimating the spatial correlation function. Overall, the proposed sparsity-based approach of this paper is useful in the sense that it does not require any model for the field of interest and can still provide a good quality prediction at low sampling rates. The model-based approach, on the other hand, can also be useful depending on the scenario. Furthermore, its probabilistic nature makes it suitable for theoretical analysis and design. For a more detailed comparison of the two approaches, as well as an integrated sparsity and model-based framework for estimating the channel spatial variations, readers are referred to [63].

4.4 A Note on the Decentralized Nature of Compressive Mapping

It should be noted that the nature of our proposed compressive mapping framework is reconstruction based on minimal sensing. Therefore, it naturally lends itself to decentralized approaches where every node can estimate the map of interest based on its own observations, as well as the observations of whichever node it can receive information from. This is particularly important in mobile cooperative networks since they typically lack a leader and the underlying graph of the network is not necessarily fully connected.

5 Conclusions

In this paper, we considered a mobile network that is tasked with building a map of the spatial variations of a parameter in its environment. We proposed a new framework that allows the nodes to build a map of the parameter of interest with a small number of measurements. By using the recent results in the area of compressive sampling, we showed how the nodes can exploit the sparse representation of the parameter of interest in order to build a map with minimal sensing, and without directly sensing a large percentage of the area. More specifically, we considered aerial mapping, mapping of the obstacles as well as mapping of the communication signal strength. In the area of obstacle mapping, we proposed a new noninvasive mapping technique for the cooperative mapping of the obstacles, based on only wireless channel measurements. Our results showed the superior performance of the proposed framework.

Acknowledgments

The author would like to thank Dr. Pradeep Sen, Soheil Darabi, and Alejandro Gonzalez-Ruiz for useful discussions. This work was supported by US National Science Foundation CAREER award #0846483. Part of this work was presented at the American Control Conference 2009 [1] and MILCOM 2008 [2].

References

[1] Y. Mostofi and P. Sen, "Compressive Cooperative Mapping in Mobile Networks," *Proc. 28th Am. Control Conf. (ACC '09)*, pp. 3397-3404, June 2009.

[2] Y. Mostofi and P. Sen, "Compressed Mapping of Communication Signal Strength," *Proc. IEEE Military Comm. Conf. (MILCOM '08)*, 2008.

[3] H. Gonzalez-Banos and J.C. Latombe, "Navigation Strategies for Exploring Indoor Environments," *The Int'l J. Robotics Research*, vol. 21, nos. 10/11, pp. 829-848, 2002.

[4] N.E. Leonard, D.A. Paley, F. Lekien, R. Sepulchre, D.M. Fratantoni, and R.E. Davis, "Collective Motion, Sensor Networks, and Ocean Sampling," *Proc. IEEE*, vol. 95, no. 1, pp. 48-74, Jan. 2007.

[5] I.I. Hussein, "Motion Planning for Multi-Spacecraft Interferometric Imaging Systems," PhD thesis, Univ. of Michigan, 2005.

[6] F. Dellaert, F. Alegre, and E.B. Martinson, "Intrinsic Localization and Mapping with 2 Applications: Diffusion Mapping and Macro Polo Localization," *Proc. IEEE Int'l Conf. Robotics and Automation,* vol. 2, pp. 2344-2349, 2003.

[7] R. Sim, G. Dudek, and N. Roy, "A Closed Form Solution to the Single Degree of Freedom Simultaneous Localisation and Map Building (SLAM) Problem," *Proc. IEEE Conf. Decision and Control,* vol. 1, pp. 191-196, 2000.

[8] P. Krauthausen, F. Dellaert, and A. Kipp, "Exploiting Locality by Nested Dissection for Square Root Smoothing and Mapping," *Proc. Robotics: Science and Systems (RSS '06),* 2006.

[9] R. Sim, G. Dudek, and N. Roy, "Online Control Policy Optimization for Minimizing Map Uncertainty during Exploration," *Proc. IEEE Int'l Conf. Robotics and Automation,* vol. 2, pp. 1758-1763, 2004.

[10] R. Gartshore, A. Aguado, and C. Galambos, "Incremental Map Building Using an Occupancy Grid for an Autonomous Monocular Robot," *Proc. Seventh Int'l Conf. Control, Automation, Robotics and Vision,* vol. 2, pp. 613-618, Dec. 2002.

[11] R. Pito, "A Solution to the Next Best View Problem for Automated Surface Acquisition," *IEEE Trans. Pattern Analysis and Machine Intelligence,* vol. 21, no. 10, pp. 1016-1030, Oct. 1999.

[12] J.J. Kuffner and S.M. LaValle, "RRT-Connect: An Efficient Approach to Single-Query Path Planning," *Proc. IEEE Int'l Conf. Robotics and Automation,* pp. 995-1001, Apr. 2000.

[13] A. Ganguli, J. Cortes, and F. Bullo, "Maximizing Visibility in Nonconvex Polygons: Nonsmooth Analysis and Gradient Algorithm Design," *Proc. Am. Control Conf.,* pp. 792-797, June 2005.

[14] R. Grabowski, P. Khosla, and H. Choset, "Autonomous Exploration via Regions of Interest," *Proc. IEEE/RSJ Int'l Conf. Intelligent Robots and Systems (IROS '03),* pp. 1691-1696, Oct. 2003.

[15] S. Martínez, "Distributed Interpolation Schemes for Field Estimation by Mobile Sensor Networks," *IEEE Trans. Control Systems Technology,* vol. 18, no. 2, pp. 491-500, Mar. 2009.

[16] J. Choi, J. Lee, and S. Oh, "Swarm Intelligence for Achieving the Global Maximum Using Spatio-Temporal Gaussian Processes," *Proc. Am. Control Conf.,* pp. 135-140, June 2008.

[17] E. Fiorelli, N.E. Leonard, P. Bhatta, D. Paley, R. Bachmayer, and D.M. Fratantoni, "Multi-AUV Control and Adaptive Sampling in Monterey Bay," *Proc. IEEE/OES Autonomous Underwater Vehicles (AUV '04),* pp. 134-147, June 2004.

[18] E. Candès, J. Romberg, and T. Tao, "Robust Uncertainty Principles: Exact Signal Reconstruction from Highly Incomplete Frequency Information," *IEEE Trans. Information Theory,* vol. 52, no. 2, pp. 489-509, Feb. 2006.

[19] D.L. Donoho, "Compressed Sensing," *IEEE Trans. Information Theory,* vol. 52, no. 4, pp. 1289-1306, Apr. 2006.

[20] C.E. Shannon, "Communication in the Presence of Noise," *Proc. Inst. of Radio Engineers,* vol. 37, no. 1, pp. 10-21, Jan. 1949.

[21] M.C. Wicks, "RF Tomography with Application to Ground Penetrating Radar," *Proc. Asilomar Conf. Signals, Systems and Computers,* pp. 2017-2022, Nov. 2007.

[22] A.M. Haimovich, R.S. Blum, and L.J. Cimini, "Mimo Radar with Widely Separated Antennas," *IEEE Signal Processing Magazine,* vol. 25, no. 1, pp. 116-129, Jan. 2008.

[23] J. Wilson and N. Patwari, "Radio Tomographic Imaging with Wireless Networks," *IEEE Trans. Mobile Computing,* vol. 9, no. 5, pp. 621-632, May 2010.

[24] M. Kanso and M. Rabbat, "Compressed RF Tomography for Wireless Sensor Networks: Centralized and Decentralized Approaches," *Proc. IEEE Int'l Conf. Distributed Computing in Sensor Systems,* June 2009.

[25] J. Tropp and A. Gilbert, "Signal Recovery from Random Measurements via Orthogonal Matching Pursuit," *IEEE Trans. Information Theory,* vol. 53, no. 12, pp. 4655-4666, Dec. 2007.

[26] US Geological Survey, http://www.usgs.gov, 2011.

[27] F. Santosa and W.W. Symes, "Linear Inversion of Band-Limited Reflection Seismograms," *SIAM J. Scientific and Statistical Computing,* vol. 7, no. 4, pp. 1307-1330, 1986.

[28] R. Gribonval and M. Nielsen, "Sparse Representations in Unions of Bases," *IEEE Trans. Information Theory,* vol. 49, no. 12, pp. 3320-3325, Dec. 2003.

[29] E.J. Candès, "The Restricted Isometry Property and Its Implications for Compressed Sensing," *Compte Rendus de l'Academie des Sciences,* vol. 346, pp. 589-592, 2008.

[30] E.J. Candès and T. Tao, "Decoding by Linear Programming," *IEEE Trans. Information Theory,* vol. 51, no. 12, pp. 4203-4215, Dec. 2005.

[31] E.J. Candès, M. Rudelson, T. Tao, and R. Vershynin, "Error Correction via Linear Programming," *Proc. IEEE 46th Ann. Symp. Foundations of Computer Science (FOCS '05),* pp. 668-681, Oct. 2005.

[32] D. Needell and R. Vershynin, "Uniform Uncertainty Principle and Signal Recovery via Regularized Orthogonal Matching Pursuit," *Foundations of Computational Math.,* vol. 9, no. 3, pp. 317-334, 2007.

[33] E.J. Candès, J. Romberg, and T. Tao, "Stable Signal Recovery from Incomplete and Inaccurate Measurements," *Comm. Pure and Applied Math,* vol. 59, no. 8, pp. 1207-1223, 2005.

[34] "Compressive Sensing Resources," http://www.dsp.ece.rice.edu/cs, 2011.

[35] M. Rudelson and R. Vershynin, "Sparse Reconstruction by Convex Relaxation: Fourier and Gaussian Measurements," *Proc. 40th Ann. Conf. Information Sciences and Systems,* pp. 207-212, Mar. 2006.

[36] *Handbook of the Geometry of Banach Spaces,* W.B. Johnson and J. Lindenstrauss, eds., vols. 1/2. Elsevier Science Ltd., 2001.

[37] S.J. Szarek, "Condition Numbers of Random Matrices," *J. Complexity,* vol. 7, no. 2, pp. 131-149, 1991.

[38] A.E. Litvak, A. Pajor, M. Rudelson, and N. Tomczak-Jaegermann, "Smallest Singular Value of Random Matrices and Geometry of Random Polytopes," *Advances in Math.,* vol. 195, no. 2, pp. 491-523, 2005.

[39] M. Duarte, M. Davenport, D. Takhar, J. Laska, T. Sun, K. Kelly, and R. Baraniuk, "Single-Pixel Imaging via Compressive Sampling," *IEEE Signal Processing Magazine,* vol. 25, no. 2, pp. 83-91, Mar. 2008.

[40] M. Lustig, D. Donoho, and J.M. Pauly, "Sparse MRI: The Application of Compressed Sensing for Rapid MR Imaging," *Magnetic Resonance in Medicine,* vol. 58, no. 6, pp. 1182-1195, Dec. 2007.

[41] M. Sheikh, O. Milenkovic, and R. Baraniuk, "Designing Compressive Sensing DNA Microarrays," *Proc. IEEE Second Int'l Workshop Computational Advances in Multi-Sensor Adaptive Processing (CAMSAP '07),* Dec. 2007.

[42] P. Sen and S. Darabi, "Compressive Dual Photography," *Eurographics,* vol. 28, pp. 609-618, 2009.

[43] S. Boyd and L. Vandenberghe, *Convex Optimization.* Cambridge Univ., 2004.

[44] S.J. Wright, R.D. Nowak, and M.A.T. Figueiredo, "Sparse Reconstruction by Separable Approximation," *Proc. IEEE Int'l Conf. Acoustics, Speech and Signal Processing,* pp. 3373-3376, Apr. 2008.

[45] M.A.T. Figueiredo, R.D. Nowak, and S.J. Wright, "Gradient Projection for Sparse Reconstruction: Application to Compressed Sensing and Other Inverse Problems," *IEEE J. Selected Topics in Signal Processing,* vol. 1, no. 4, pp. 586-597, Dec. 2007.

[46] Y. Nesterov, "Gradient Methods for Minimizing Composite Objective Function," discussion paper, Center for Operations Research and Econometrics (CORE), 2007.

[47] P. Patel and J. Holtzman, "Analysis of a Simple Successive Interference Cancellation Scheme in a DS/CDMA System," *IEEE J. Selected Areas in Comm.,* vol. 12, no. 5, pp. 796-807, June 1994.

[48] Y. Mostofi and S.A. Mujtaba, "Asynchronous Code Acquisition and Channel Estimation for Uplink DS-CDMA Systems," technical report, Lucent Technologies, Sept. 1999.

[49] R. Berinde, A.C. Gilbert, P. Indyk, H. Karloff, and M.J. Strauss, "Combining Geometry and Combinatorics: A Unified Approach to Sparse Signal Recovery," *Proc. 46th Ann. Allerton Conf. Comm., Control, and Computing,* pp. 798-805, Sept. 2008.

[50] P. Sen and S. Darabi, "Compressive Rendering: A Rendering Application of Compressed Sensing," *IEEE Trans. Visualization and Computer Graphics,* vol. 17 no. 4, pp. 487-499, April 2011.

[51] A.C. Kak and M. Slaney, *Principles of Computerized Tomographic Imaging.* IEEE, 1988.

[52] R. Ketcham, *Computed Tomography for Paleontology and Geology.* Cambridge Univ., 2004.

[53] R. Ng, "Fourier Slice Photography," *Proc. ACM SIGGRAPH,* pp. 735-744, 2005.

[54] A. Goldsmith, *Wireless Communications.* Cambridge Univ., 2005.

[55] W.C. Jakes, *Microwave Mobile Communications.* Wiley-IEEE, 1994.

[56] Y. Mostofi, A. Gonzales-Ruiz, A. Ghaffarkhah, and D. Li, "Characterization and Modeling of Wireless Channels for Networked Robotic and Control Systems—A Comprehensive Overview," *Proc. IEEE/RSJ Int'l Conf. Intelligent Robots and Systems (IROS '09),* pp. 4849-4854, Oct. 2009.

[57] "ℓ_1 Magic Toolbox," http://www.acm.caltech.edu/l1magic, 2011.

[58] Y. Mostofi, "Compressive Cooperative Obstacle/Object Mapping and See-Through Capabilities in Robotic Networks," in preparation for submission, 2011.
[59] Y. Mostofi and A. Gonzalez-Ruiz, "Compressive Cooperative Obstacle Mapping in Mobile Networks," *Proc. IEEE MILCOM,* pp. 524-530, Nov. 2010.
[60] W.M. Smith, "Urban Propagation Modeling for Wireless Systems," PhD thesis, Stanford Univ., 2004.
[61] Y. Mostofi, M. Malmirchegini, and A. Ghaffarkhah, "Estimation of Communication Signal Strength in Robotic Networks," *Proc. IEEE Int'l Conf. Robotics and Automation (ICRA '10),* pp. 1946-1951, May 2010.
[62] M. Malmirchegini and Y. Mostofi, "On the Spatial Predictability of Communication Channels," *IEEE Trans. Wireless Comm.,* to appear, 2011.
[63] M. Malmirchegini and Y. Mostofi, "An Integrated Sparsity and Model-Based Probabilistic Framework for Estimating the Spatial Variations of Communication Channels," *Physical Comm.,* Special Issue on Compressive Sensing in Communications, to appear, 2011.

Yasamin Mostofi received the BS degree in electrical engineering from the Sharif University of Technology, Tehran, Iran, in 1997, and the MS and PhD degrees in the area of wireless communication systems from Stanford University, California, in 1999 and 2004, respectively. She is currently an assistant professor in the Department of Electrical and Computer Engineering at the University of New Mexico. Prior to that, she was a postdoctoral scholar in control and dynamical systems at the California Institute of Technology from 2004 to 2006. Her current research lies at the intersection of the two areas of communications and control/robotics in mobile sensor networks. Current research projects include communication-aware navigation and decision making in robotic networks, compressive sensing and control, obstacle mapping, robotic routers, and cooperative information processing. Dr. Mostofi is the recipient of the Presidential Early Career Award for Scientists and Engineers (PECASE) and the US National Science Foundation (NSF) CAREER award. She also received the Bellcore fellow-advisor award from the Stanford Center for Telecommunications in 1999. She won the 2008-2009 Electrical and Computer Engineering Distinguished Researcher Award from the University of New Mexico. She has served on the Control Systems Society conference editorial board since 2008. She is a member of the IEEE.